Available online at www.sciencedirect.com
ScienceDirect
Journal of Power Sources 171 (2007) 412–423
JOURNAL OF POWER SOURCES
www.elsevier.com/locate/jpowsour

A lumped parameter model of the polymer electrolyte fuel cell

Keonyup Chu [a], Junghwan Ryu [a], Myoungho Sunwoo [b,*]

[a] *Department of Automotive Engineering, Graduate School, Hanyang University, 17 Haengdang-dong, Seongdong-gu, Seoul 133-791, Korea*
[b] *Department of Automotive Engineering, Hanyang University, 17 Haengdang-dong, Seongdong-gu, Seoul 133-791, Korea*

Received 30 March 2007; accepted 17 May 2007
Available online 23 June 2007

Abstract

A model of a polymer electrolyte fuel cell (PEFC) is developed that captures dynamic behaviour for control purposes. The model is mathematically simple, but accounts for the essential phenomena that define PEFC performance. In particular, performance depends principally on humidity, temperature and gas pressure in the fuel cell system. To simulate accurately PEFC operation, the effects of water transport, hydration in the membrane, temperature, and mass transport in the fuel cells system are simultaneously coupled in the model. The PEFC model address three physically distinctive fuel cell components, namely, the anode channel, the cathode channel, and the membrane electrode assembly (MEA). The laws of mass and energy conservation are applied to describe each physical component as a control volume. In addition, the MEA model includes a steady-state electrochemical model, which consists of membrane hydration and the stack voltage models.

Keywords: Polymer electrolyte fuel cell; Model; Dynamics; Lumped parameter

1. Introduction

Fuel cells may be used to replace the conventional internal combustion engine in vehicles because of their capacity to achieve a high efficiency. In particular, they are being considered as suitable potential power sources for zero-emission vehicles (ZEVs). Most automobile manufacturers consider the fuel cell electric vehicle to be logical successor to the hybrid electric vehicle, and major automotive companies have already presented cars that use fuel cells as the power plant. Among the various types of fuel cells, the polymer electrolyte fuel cell (PEFC) has the greatest potential for use in automotive applications because of its low operating temperature, solid-type electrolyte, high efficiency, and high power density [1]. PEFC technology has now reached the testing and demonstration phase, and engineering development and optimization are vital for realization of commercial products [2]. It is especially necessary for PEFC technologies to be developed in tandem with dedicated control systems which, in turn, requires effective modelling of technology. The operation and physical phenomena within the PEFC system can be clearly understood through this modelling process. The knowledge acquired through the modelling the PEFC and simulations using this model can also be applied to the design of control systems for the PEFC.

2. Model setup and assumption

Although the PEFC model developed in this study is mathematically simple, it accounts for the essential phenomena that define PEFC performance. The performance of the PEFC depends principally on the properties of the membrane and the thermodynamics of the gas in the fuel cell system, and the model emphasizes these elements accordingly. The PEFC system consists of the three physically distinct parts shown in Fig. 1, namely, the anode channel, the cathode channel, and the membrane electrode assembly (MEA) [3]. The mass and energy conservation laws are applied to describe each physical component as a control volume. In addition, the MEA model contains a steady-state electrochemical model that consists of a membrane hydration model and a stack voltage model [4]. This model is the lumped parameter model, so spatial variations of the temperature, pressure, and concentration are ignored. Dynamics for flow and temperature, however, are included. The inputs are electric current, mass flow rate, humidity, and the

* Corresponding author. Tel.: +82 2 2290 0453; fax: +82 2 2297 5495.
E-mail addresses: acehev@hanyang.ac.kr (K. Chu), yesican@hanyang.ac.kr (J. Ryu), msunwoo@hanyang.ac.kr (M. Sunwoo).

0378-7753/$ – see front matter © 2007 Published by Elsevier B.V.
doi:10.1016/j.jpowsour.2007.05.108

Nomenclature

a	activity of water
A	fuel cell active area (cm^2)
$c_{AN,V}$	anode water concentration
$c_{CA,V}$	cathode water concentration
c_p	specific heat at constant pressure ($kJ\,kg^{-1}\,K$)
c_v	specific heat at constant volume ($kJ\,kg^{-1}\,K$)
D_W	diffusion coefficient of water concentration
E^{CV}	internal energy of control volume (kJ)
E^{Nerst}	reversible open circuit voltage (V)
F	Faraday constant (C)
ΔH^{react}	enthalpy of reaction ($kJ\,kmol^{-1}$)
(hA)	heat convection coefficient ($kJ\,K^{-1}$)
I	stack current (A)
i	stack current density ($A\,cm^{-2}$)
k	effective permeability (cm^2)
k_{sat}	permeability (cm^2)
K	nozzle coefficient ($kg\,s^{-1}\,atm$)
m	mass (kg)
$\dot{m}$	mass flow rate ($kg\,s^{-1}$)
M	molecular mass ($kg\,kmol^{-1}$)
N	molar flux ($kmol\,m^{-2}s^{-}$)
n_{cell}	number of cell
n_d	electro-osmotic drag coefficient
p	pressure (kPa)
$\dot{Q}$	rate of heat transfer (kW)
T	temperature (K)
T_0	standard temperature (K)
t_M	thickness of the membrane (cm)
V	channel volume (cm^3)
$\bar{V}$	molar volume (cm^3)
$\dot{W}$	electric power (kW)
x	mole fraction

Greek letters

η_{act}	activation loss (V)
η_{ohmic}	Ohmic loss (V)
η_{conc}	concentration loss (V)
λ	water content
$\rho_{M,dry}$	membrane dry density ($kg\,cm^{-3}$)
σ_m	membrane conductivity

Subscripts

AMB	ambient condition
AN	anode
CA	cathode
conc	concentration
d	electro-osmotic drag
H_2	hydrogen gas
L	liquid type of water
m	membrane
M	membrane electrode assembly
N_2	nitrogen gas
O_2	oxygen gas
ohmic	Ohmic
prod	production
sat	saturation condition
V	vapor type of water
W	water

Superscripts

ave	average
conv	convection
diff	diffusion
I	inlet
latent	latent
O	outlet
osmotic	electro-osmotic drag
react	reaction
trans	translation

temperatures of the supplied gas and coolant. Some states which cannot be directly calculated by input variables, such as the pressure, humidity, concentration and temperature of gas in the channel, are determined by the dynamics of the fuel cell system. The output variables of a fuel cell system such as exhaust temperature, exhaust mass flow rate, and the stack voltage are considered to be functions of the states and the input variables. The main assumptions of this PEFC model are as follows:

- the gases are ideal and well-mixed in the channel,
- there is no pressure gradient in the channel,
- there is no temperature gradient in the channel,
- there is no current gradient across the membrane,
- the MEA temperature is uniform,
- the mole fractions in the channel and exhaust gas are equal,
- the temperatures of the condensed water and the MEA are equal,
- the radiation heat-transfer effect is negligible.

3. Mathematical model

3.1. Review of thermodynamics

3.1.1. Saturation vapour properties

Water is always accompanied with the dry gas in the channel because of hydration of the membrane and the generation of water due to the chemical reaction. So the phase of water in the PEFC is important factor in determining the thermodynamic states such as pressure, and temperature. The saturation vapor pressure $p_{sat}(T)$ (kPa) according to vapour temperature is modelled using the table of saturated water [5].

$$\log_{10} p_{sat}(T) = -20.92 + 0.143T - 3.39 \times 10^{-4}T^2 + 3.85 \times 10^{-7}T^3 - 1.69 \times 10^{-10}T^4 \quad (1)$$

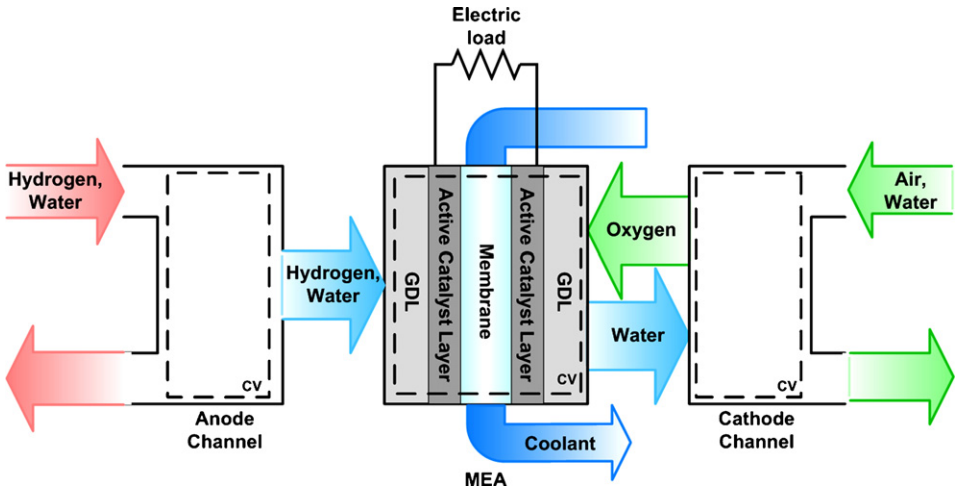

Fig. 1. PEFC model structure.

where T is the vapour temperature (K). The mass of saturation vapour is determined by the Ideal Gas Law.

$$m_{\mathrm{V,sat}} = \frac{p_{\mathrm{sat}} V}{M_{\mathrm{H_2O}} \bar{R} T} \tag{2}$$

The derivative of $m_{\mathrm{V,sat}}$ is given by:

$$\frac{\mathrm{d}m_{\mathrm{V,sat}}}{\mathrm{d}t} = \frac{\partial m_{V,\mathrm{sat}}}{\partial T}\frac{\mathrm{d}T}{\mathrm{d}t} + \frac{\partial m_{V,\mathrm{sat}}}{\partial p_{\mathrm{sat}}}\frac{\mathrm{d}p_{\mathrm{sat}}}{\mathrm{d}t} \tag{3}$$

where $\partial m_{\mathrm{V,sat}}/\partial T = -(p_{\mathrm{sat,V}}/R)T^{-2}$ and $\partial m_{\mathrm{V,sat}}/\partial p_{\mathrm{sat}} = V/(RT)$. The above relationship requires the determination of the time derivative of $p_{\mathrm{sat}}(T)$.

$$\frac{\mathrm{d}p_{\mathrm{sat}}}{\mathrm{d}t} = p_{\mathrm{sat}} \ln 10 \frac{\mathrm{d}T}{\mathrm{d}t}\frac{\mathrm{d}(\log_{10} p_{\mathrm{sat}})}{\mathrm{d}T} \tag{4}$$

3.1.2. Latent heat

The latent heat effect is a crucial factor that affects the heat transfer in the PEFC system, because a large quantity of water is generated by chemical reactions and is changed between the liquid and vapour phases according to the dew point and the vapour pressure. The heat of evaporation or condensation H^{vapor} may be estimated as a function of temperature by following Eq. [6]:

$$H^{\mathrm{vapor}} = 45,070 - 41.9T + 3.44 \times 10^{-3}T^2 + 2.54 \times 10^{-6}T^3 - 8.98 \times 10^{-10}T^4 \tag{5}$$

3.2. Anode channel model

Hydrogen and vapour enter the anode channel (Fig. 2), some of which diffuses through the gas-diffusion layer (GDL) and some of which leaves the channel [4]. Heat transfer from the MEA to the gas in the channel affects the temperature and pressure of the gas in the anode channel. The anode channel is considered as a control volume in describing these phenomena.

3.2.1. Anode channel flow model

The mass continuity of hydrogen and water is used to develop the flow model in the anode control volume.

$$\begin{aligned}\frac{\mathrm{d}m_{\mathrm{AN,H_2}}}{\mathrm{d}t} &= \dot{m}^{\mathrm{I}}_{\mathrm{AN},H_2} - \dot{m}^{\mathrm{O}}_{\mathrm{AN,H_2}} - \dot{m}^{\mathrm{react}}_{\mathrm{H_2}} \\ \frac{\mathrm{d}m_{\mathrm{AN,W}}}{\mathrm{d}t} &= \dot{m}^{\mathrm{I}}_{\mathrm{AN,V}} - \dot{m}^{\mathrm{O}}_{\mathrm{AN,V}} - \dot{m}^{\mathrm{trans}}_{\mathrm{V}}\end{aligned} \tag{6}$$

The water inside the anode control volume is one of phases, vapour or liquid, depending on the amount of maximum vapour $m_{\mathrm{AN,V,sat}}$ [5], which is in turn determined by the saturation pressure $p_{\mathrm{AN,V,sat}}$ corresponding to the temperature of the anode gas.

If $m_{\mathrm{AN,W}} > m_{\mathrm{AN,V,sat}}$:

$$\begin{aligned} m_{\mathrm{AN,V}} &= m_{\mathrm{AN,V,sat}} \\ \dot{m}_{\mathrm{AN},V} &= \dot{m}_{\mathrm{AN,V,sat}} \\ m_{\mathrm{AN,L}} &= m_{\mathrm{AN,W}} - m_{\mathrm{AN,V}} \\ \dot{m}_{\mathrm{AN,L}} &= -\dot{m}^{\mathrm{vapor}}_{\mathrm{AN,V}} = \dot{m}_{\mathrm{AN,W}} - \dot{m}_{\mathrm{AN,V}} \end{aligned} \tag{7}$$

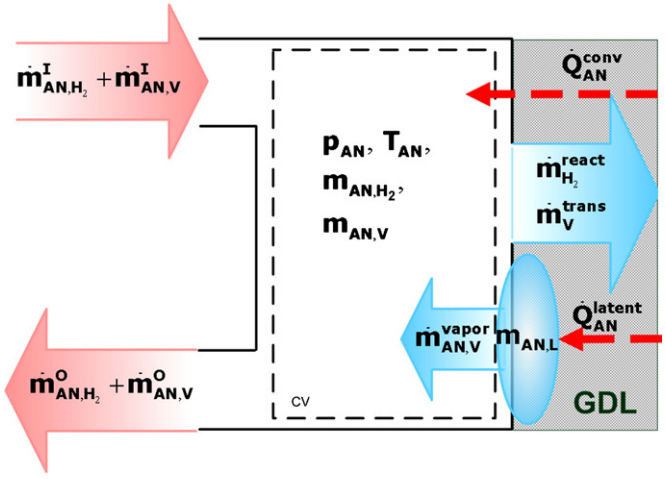

Fig. 2. Anode channel model.

Or if $m_{AN,W} \leq m_{AN,V,sat}$:

$$\begin{aligned} m_{AN,V} &= m_{AN,W} \\ \dot{m}_{AN,V} &= \dot{m}_{AN,W} \\ m_{AN,L} &= 0 \\ \dot{m}_{AN,L} &= -\dot{m}_{AN,V}^{vapor} = 0 \end{aligned} \tag{8}$$

The mass flow rate of the anode exhaust gas $\dot{m}_{AN}^{O}$ is assumed to be proportional to the pressure difference, i.e.,

$$\dot{m}_{AN}^{O} = K_{AN}(p_{AN} - p_{AMB}) \tag{9}$$

It is assumed that the mole fractions of the outlet flows are the same as those of the gas in the anode control volume. Using anode channel pressure and mass fractions, hydrogen flow and water flow at the outlet can be given by:

$$\dot{m}_{AN,i}^{O} = \frac{M_i x_{AN,i} K_{AN}(p_{AN} - p_{AMB})}{\sum_j M_j x_{AN,j}} \quad i = H_2, H_2O \tag{10}$$

Faraday's law is used to calculate the mass flow rate of hydrogen consumption in reaction [7]. The mass flow rate is determined according to:

$$\dot{m}_{H_2}^{react} = M_{H_2} n_{cell} \frac{I}{2F} \tag{11}$$

3.2.2. Anode thermal model

The energy rate balance for the anode control volume is:

$$\frac{dE_{AN}^{CV}}{dt} = \dot{Q}_{AN}^{conv} + \sum \dot{m}_{AN}^{I} h_{AN}^{I} - \sum \dot{m}_{AN}^{O} h_{AN}^{O} \tag{12}$$

where $\dot{Q}_{AN}^{conv}$ is the heat transfer rate across the MEA to the anode channel, and $\sum \dot{m}_{AN}^{I} h_{AN}^{I} - \sum \dot{m}_{AN}^{O} h_{AN}^{O}$ is the net energy rate by the mass flow. The convective heat transfer $\dot{Q}_{AN}^{conv}$ is caused by the temperature difference between the MEA and the anode [3,8,9]:

$$\dot{Q}_{AN}^{conv} = (hA)_{AN}(T_M - T_{AN}) \tag{13}$$

where $(hA)_{AN}$ is the heat convection coefficient of the anode channel. The net energy rate by the mass flow is given by:

$$\begin{aligned} &\sum \dot{m}_{AN}^{I} h_{AN}^{I} - \sum \dot{m}_{AN}^{O} h_{AN}^{O} \\ &= \dot{m}_{AN,H_2}^{I} c_{p,H_2}(T_{AN}^{I} - T_0) - \dot{m}_{AN,H_2}^{O} c_{p,H_2}(T_{AN} - T_0) \\ &\quad -\dot{m}_{AN,H_2}^{react} c_{p,H_2}(T_{AN} - T_0) + \dot{m}_{AN,V}^{I} c_{p,V}(T_{AN}^{I} - T_0) \\ &\quad -\dot{m}_{AN,V}^{O} c_{p,V}(T_{AN} - T_0) + \dot{m}_{AN,V}^{vapor} c_{p,V}(T_{AN,V}^{vapor} - T_0) \\ &\quad -\dot{m}_{V}^{trans} c_{p,V}(T_{AN,V}^{trans} - T_0) \end{aligned} \tag{14}$$

where $T_{AN,V}^{vapor}$ represents the temperature of the vapourized water or the temperature of the condensed water in the anode channel, and $T_{AN,V}^{trans}$ represents the temperature of the vapor moving from the MEA to the anode channel or from the anode channel to the MEA. $T_{AN,V}^{vapor}$ and $T_{AN,V}^{trans}$ are determined by the sign of $\dot{m}_{AN,V}^{vapor}$ and $\dot{m}_{V}^{trans}$. If $\dot{m}_{AN,V}^{vapor}$ is positive, $T_{AN,V}^{vapor}$ is the same; otherwise $T_{AN,V}^{vapor}$ is T_{AN}. $T_{AN,V}^{trans}$ is T_{AN} if $\dot{m}_{V}^{trans}$ is positive and T_M if $\dot{m}_{V}^{trans}$ is negative. The internal energy of the anode control volume can be expressed as follows:

$$E_{AN}^{CV} = (m_{AN,H_2} c_{v,H_2} + m_{AN,V} c_{v,V})(T_{AN} - T_0) \tag{15}$$

Using Eqs. (12) and (15), the time rate of the temperature for anode control volume can be expressed as follows:

$$\frac{dT_{AN}}{dt} = \frac{\dot{E}_{AN}^{CV} - (\dot{m}_{AN,H_2} c_{v,H_2} + \dot{m}_{AN,V} c_{v,V})(T_{AN} - T_0)}{m_{AN,H_2} c_{v,H_2} + m_{AN,V} c_{v,V}} \tag{16}$$

3.3. Cathode channel model

The mass flow, energy flow, and gas pressure in the cathode control volume are similar to those in the anode control volume. Flows of oxygen, nitrogen and water in the cathode are considered as in Fig. 3. Oxygen molecules are involved in the chemical reaction and move to the membrane and react with protons. As a result, liquid water is produced at the catalyst of the cathode side of the MEA [10,11]. Moreover, heat transfer by temperature gradient to the MEA affects the temperature and pressure of the gas in the cathode channel.

3.3.1. Cathode flow model

The cathode flow model describes the flow of air and vapour inside the cathode channel. The mass conservation law and the Ideal Gas Law are used to determine the pressure of the gas in the cathode control volume.

$$\begin{aligned} \dot{m}_{CA,O_2} &= \dot{m}_{CA,O_2}^{I} - \dot{m}_{CA,O_2}^{O} - \dot{m}_{O_2}^{react} \\ \dot{m}_{CA,N_2} &= \dot{m}_{CA,N_2}^{I} - \dot{m}_{CA,N_2}^{O} \\ \dot{m}_{CA,W} &= \dot{m}_{CA,V}^{I} - \dot{m}_{CA,V}^{O} + \dot{m}_{V}^{trans} + \dot{m}_{L}^{prod} \end{aligned} \tag{17}$$

The behaviour of the water inside the cathode channel is somewhat different from that or of the water inside the anode channel due to the production of water reacting at the cathode side of the membrane close to the GDL. It is assumed that all of the water produced by the chemical reaction is liquid. The

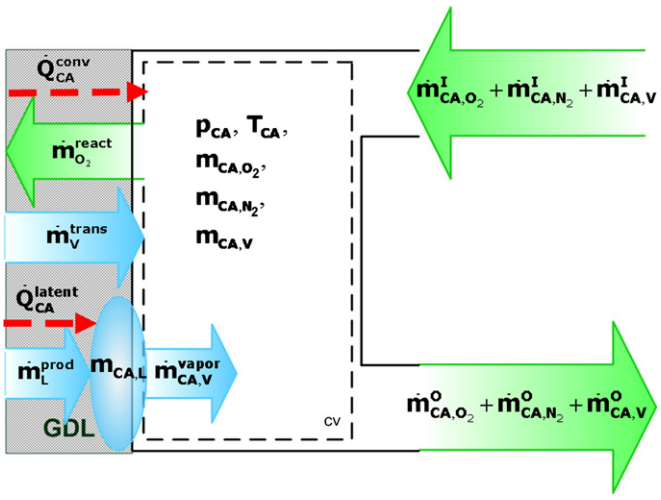

Fig. 3. Cathode channel model.

water inside the cathode channel is in one of two phases, i.e., vapour and liquid, and depends on $m_{CA,V,sat}$, which is in turn determined by the saturation pressure [5].

If $m_{CA,W} > m_{CA,V,sat}$,

$$\begin{aligned} m_{CA,V} &= m_{CA,V,sat} \\ \dot{m}_{CA,V} &= \dot{m}_{CA,V,sat} \\ m_{CA,L} &= m_{CA,W} - m_{CA,V} \\ \dot{m}_{CA,L} &= \dot{m}_{CA,W} - \dot{m}_{CA,V} \\ \dot{m}^{vapor}_{CA,V} &= \dot{m}_{CA,V} + \dot{m}^{prod}_{CA,L} - \dot{m}_{CA,W} \end{aligned} \tag{18}$$

Else if $m_{CA,W} \le m_{CA,V,sat}$,

$$\begin{aligned} m_{CA,V} &= m_{CA,W} \\ \dot{m}_{CA,V} &= \dot{m}_{CA,W} \\ m_{CA,L} &= 0 \\ \dot{m}_{CA,L} &= \dot{m}_{CA,W} - \dot{m}_{CA,V} = 0 \\ \dot{m}^{vapor}_{CA,V} &= \dot{m}^{prod}_{CA,L} \end{aligned} \tag{19}$$

It is assumed that the mole fractions of the outlet flows are the same as those of gas in the cathode control volume. The cathode outlet flow of each species can be expressed using pressure difference and mass fractions [3]:

$$\dot{m}^{O}_{CA,i} = \frac{K_{CA} M_i x_{CA,i} (p_{CA} - p_{AMB})}{\sum_i M_i x_{CA,i}} \quad i = O_2,\ N_2,\ H_2O \tag{20}$$

The mass flow rate of oxygen for the chemical reaction is determined by the stack current [7], i.e.,

$$\dot{m}^{react}_{O_2} = M_{O_2} n_{cell} \frac{I}{4F} \tag{21}$$

3.3.2. Cathode thermal model

The energy rate balance of the cathode control volume is given by:

$$\frac{dE^{CV}_{CA}}{dt} = \dot{Q}^{conv}_{CA} + \sum \dot{m}^{I}_{CA} h^{I}_{CA} - \sum \dot{m}^{O}_{CA} h^{O}_{CA} \tag{22}$$

where $\dot{Q}^{conv}_{CA}$ is the rate of heat transfer across the MEA to the cathode channel, $\sum \dot{m}^{I}_{CA} h^{I}_{CA} - \sum \dot{m}^{O}_{CA} h^{O}_{CA}$ is the net energy rate by mass flows. Heat convection $\dot{Q}^{conv}_{CA}$ is caused by a difference in the temperature between the MEA and the cathode [3,8,9]:

$$\dot{Q}^{conv}_{CA} = (hA)_{CA}(T_M - T_{CA}) \tag{23}$$

where $(hA)_{CA}$ is the heat convection coefficient of the cathode channel. The net energy rate by mass flows is given by:

$$\begin{aligned} &\sum \dot{m}^{I}_{CA} h^{I}_{CA} - \sum \dot{m}^{O}_{CA} h^{O}_{CA} \\ &= \dot{m}^{I}_{CA,O_2} c_{p,O_2} (T^{I}_{CA} - T_0) - \dot{m}^{O}_{CA,O_2} c_{p,O_2} (T_{CA} - T_0) \\ &\quad - \dot{m}^{react}_{CA,O_2} c_{p,O_2} (T_{CA} - T_0) + \dot{m}^{I}_{CA,N_2} c_{p,N_2} (T^{I}_{CA} - T_0) \\ &\quad - \dot{m}^{O}_{CA,N_2} c_{p,N_2} (T_{CA} - T_0) + \dot{m}^{I}_{CA,V} c_{p,V} (T^{I}_{CA} - T_0) \\ &\quad - \dot{m}^{O}_{CA,V} c_{p,V} (T_{CA} - T_0) + \dot{m}^{trans}_{V} c_{p,V} (T^{trans}_{CA,V} - T_0) \\ &\quad + \dot{m}^{vapor}_{CA,V} c_{p,V} (T^{vapor}_{CA,V} - T_0) \end{aligned} \tag{24}$$

where $T^{vapor}_{CA,V}$ represents the temperature of the vapourized water or that of the condensed water in the cathode channel, and $T^{trans}_{CA,V}$ represents the temperature of the vapour moving between the MEA and the cathode channel or from the cathode channel to the MEA. $T^{vapor}_{CA,V}$ and $T^{trans}_{CA,V}$ is determined by the signs of $\dot{m}^{vapor}_{CA,V}$ and $\dot{m}^{trans}_{V}$. If $\dot{m}^{vapor}_{CA,V}$ is positive, $T^{vapor}_{CA,V}$ is same as T_M. Otherwise, $T^{vapor}_{CA,V}$ is T_{CA}. $T^{trans}_{CA,V}$ is T_M if $\dot{m}^{trans}_{V}$ is positive and T_{CA} if $\dot{m}^{trans}_{V}$ is negative. The internal energy of the cathode control volume can be expressed as follows:

$$\begin{aligned} E^{CV}_{CA} = \{&(m_{CA,O_2} c_{v,O_2} + m_{CA,N_2} c_{v,N_2} + m_{CA,V} c_{v,V}) \\ &\times (T_{CA} - T_0)\} \end{aligned} \tag{25}$$

Using Eqs. (22) and (25), the time rate of the temperature for cathode control volume can be expressed as follows:

$$\frac{dT_{CA}}{dt} = \frac{\dot{E}^{CV}_{CA} - (\dot{m}_{CA,O_2} c_{v,O_2} + \dot{m}_{CA,N_2} c_{v,N_2} + \dot{m}_{CA,V} c_{v,V})(T_{CA} - T_0)}{m_{CA,O_2} c_{v,O_2} + m_{CA,N_2} c_{v,N_2} + m_{CA,V} c_{v,V}} \tag{26}$$

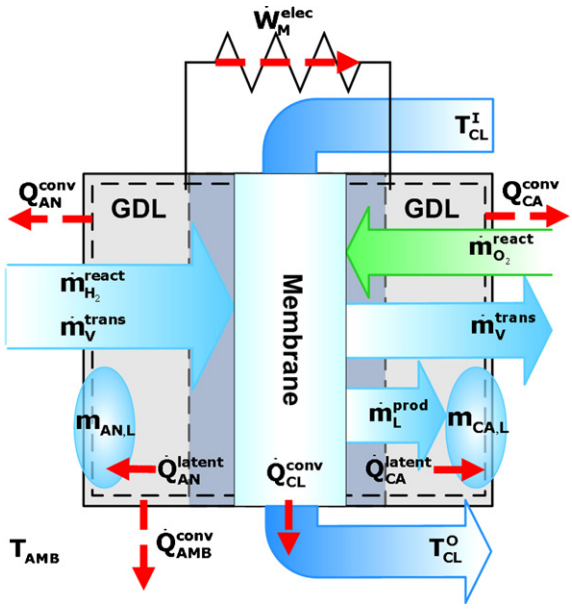

Fig. 4. Membrane electrode assembly model.

3.4. Membrane electrode assembly model

Three sub-models included in the MEA model are the membrane hydration model, the stack voltage model, and the MEA thermal model. Simplified features of the MEA are shown in Fig. 4, which illustrates the energy and the mass balances within the MEA control volume.

3.4.1. Membrane hydration model

Water molecules are dragged across the membrane from the anode to the cathode by the protons. This phenomenon is called electro-osmotic drag. There is a water concentration gradient across the membrane caused by the difference in the humidity between the anode and cathode flows and which in turn causes diffusion. The pressure gradient across the membrane causes the convection within the pores of the membrane. By combining the three water transports, the water flow across the membrane $\dot{m}_{\mathrm{V}}^{\mathrm{trans}}$ can be written as follows [5,10–14]:

$$\dot{n}_{\mathrm{V}}^{\mathrm{trans}} = \left(n_{\mathrm{d}} \frac{i}{F} - D_{\mathrm{w}} \frac{(c_{\mathrm{CA,V}} - c_{\mathrm{AN,V}})}{t_{\mathrm{M}}} - \frac{k}{\mu \bar{V}_0} \frac{(P_{\mathrm{CA}} - P_{\mathrm{AN}})}{t_{\mathrm{M}}} \right)$$
$$\dot{m}_{\mathrm{V}}^{\mathrm{trans}} = n_{\mathrm{cell}} \times A \times M_{\mathrm{H_2O}} \times \dot{n}_{\mathrm{V}}^{\mathrm{trans}} \tag{27}$$

where A is the active area of the fuel cell. The membrane water content and the electro-osmotic and diffusion coefficients can be calculated using the activities of the water in the anode and the cathode [4,5]. It is assumed that the temperature of water adjacent to the membrane is the same as that of the MEA. So the activities of water at the anode and the cathode sides of the membrane are determined by:

$$a_{\mathrm{AN}} = \frac{x_{\mathrm{AN,W}} p_{\mathrm{AN}}}{p^{\mathrm{sat}}(T_{\mathrm{M}})}, \qquad a_{\mathrm{CA}} = \frac{x_{\mathrm{CA,W}} p_{\mathrm{CA}}}{p^{\mathrm{sat}}(T_{\mathrm{M}})}$$
$$a_{\mathrm{ave}} = \frac{a_{\mathrm{AN}} + a_{\mathrm{CA}}}{2} \tag{28}$$

The membrane water content λ_i is calculated from water activities a_i [5]:

$$\lambda_i = \begin{cases} 0.043 + 17.81 a_i - 39.85 a_i^2 + 36.0 a_i^3, & 0 < a_i \le 1 \\ 14 + 1.4(a_i - 1), & 1 < a_i \end{cases}$$
$$i = \mathrm{AN, CA} \tag{29}$$

The average membrane water content λ_{ave} is the arithmetic mean of the water content. The electro-osmotic drag coefficient n_{d} and the water diffusion coefficient D_{W} are calculated from λ_{ave} as follows [4,5]:

$$n_{\mathrm{d}} = \frac{2.5}{22} \lambda_{\mathrm{ave}}, \qquad D_{\mathrm{W}} = D_\lambda \exp\left(2416 \left(\frac{1}{303} - \frac{1}{T_{\mathrm{M}}} \right) \right) \tag{30}$$

The water concentrations at the membrane surfaces on the anode and cathode sides are functions of the membrane water content [5]:

$$c_{\mathrm{AN,V}} = \frac{\rho_{\mathrm{M,dry}}}{M_{\mathrm{M,dry}}} \lambda_{\mathrm{AN}}, \qquad c_{\mathrm{CA,V}} = \frac{\rho_{\mathrm{M,dry}}}{M_{\mathrm{M,dry}}} \lambda_{\mathrm{CA}} \tag{31}$$

For the liquid water flow through the membrane, Darcy's law is used to express an influence of the pressure gradient. In Eq. (27), the water flux caused by the pressure gradient is proportional to the effective permeability and the inverse of viscosity of water. The effective permeability is a function of the absolute permeability and the water volume fraction in the membrane. The effective permeability can be expressed by [13]:

$$k = k_{\mathrm{sat}} \left(\frac{f}{f_{\mathrm{L}}} \right)^2 \tag{32}$$

where f_{L} is the maximum water volume fraction and f is the water volume fraction. The water volume fraction is expressed by [13]:

$$f = \frac{\lambda \bar{V}_{\mathrm{W}}}{\bar{V}_{\mathrm{m}} + \lambda \bar{V}_{\mathrm{W}}}, \tag{33}$$

where $\bar{V}_{\mathrm{m}}$ is the partial molar volume of the membrane and $\bar{V}_{\mathrm{W}}$ is the molar volume of water [13].

$$\bar{V}_{\mathrm{W}} = \frac{M_{\mathrm{W}}}{\rho_{\mathrm{W}}}, \qquad \bar{V}_{\mathrm{m}} = \frac{M_{\mathrm{M,dry}}}{\rho_{\mathrm{M,dry}}} \tag{34}$$

3.4.2. Stack voltage model

The voltage is a function of stack current, cathode pressure, reactant partial pressure, MEA temperature, and membrane humidity. The cell voltage is determined by the combination of E_{Nerst}, η_{act}, η_{ohmic}, and η_{conc} [5,15–16]:

$$V_{\mathrm{cell}} = E_{\mathrm{Nernst}} - \eta_{\mathrm{act}} - \eta_{\mathrm{ohmic}} - \eta_{\mathrm{conc}} \tag{35}$$

The voltage E_{Nernst} is the reversible open-circuit voltage, which is derived from the change in Gibbs free energy [4,5,7].

$$E_{\mathrm{Nernst}} = 1.229 - (8.5 \times 10^{-4})(T_{\mathrm{M}} - 298.15) + (4.308 \times 10^{-5}) T_{\mathrm{M}} (\ln p_{\mathrm{AN,H_2}} + 0.5 \ln p_{\mathrm{CA,O_2}}) \tag{36}$$

Activation losses are caused by the need to move electrons and to break and form chemical bonds at the anode and cathode [5]. The activation losses are described by:

$$\eta_{\mathrm{act}} = \upsilon_0 + \upsilon_a (1 - e^{-c_1 i}) \tag{37}$$

Ohmic losses are caused by the resistance of the membrane to the transfer of protons and resistance to the flow of electrons through the electrode material and various interconnections. The resistance due to the movement of electrons is ignored in this model. The Ohmic losses are proportional to the current density [5]:

$$\eta_{\mathrm{ohmic}} = \frac{t_{\mathrm{m}}}{\sigma_{\mathrm{m}}} i, \quad \sigma_{\mathrm{m}} = (b_{11} \lambda_{\mathrm{m}} - b_{12}) \exp\left(b_2 \left(\frac{1}{303} - \frac{1}{T_{\mathrm{M}}} \right) \right) \tag{38}$$

where σ_{m} is the membrane conductivity. Concentration losses result from the reduction in concentration caused by insufficient quantities of reactant to the electrode surface [5], i.e.,

$$\eta_{\mathrm{conc}} = i \left(c_2 \frac{i}{i_{\max}} \right)^{c_3}, \quad i_{\max} = 2.2 \tag{39}$$

3.4.3. MEA thermal model

The energy rate balance of the MEA control volume can be expressed as:

$$\frac{dE_M^{CV}}{dt} = \dot{Q}_M^{CV} + \dot{W}_M^{elec} + \sum \dot{m}_M^I h_M^I - \sum \dot{m}_M^O h_M^O \quad (40)$$

where $\dot{Q}_M^{CV}$ is the rate of heat transfer within the MEA, $\dot{W}_M^{elec}$ is the electric power generated by the PEFC, $\dot{m}_M^I h_M^I$ is the thermal energy transfer rate due to flows coming into the MEA, and $\dot{m}_M^O h_M^O$ is the thermal energy transfer rate due to flows going out of the MEA. The heat transfer rates in the MEA consist of the seven terms [3,6,8,11]:

$$\dot{Q}_M^{CV} = \dot{Q}_M^{react} - \dot{Q}_{AN}^{conv} - \dot{Q}_{CA}^{conv} - \dot{Q}_{CL}^{conv} - \dot{Q}_{AMB}^{conv} - \dot{Q}_{AN}^{latent} - \dot{Q}_{CA}^{latent} \quad (41)$$

$$\dot{Q}_M^{react} = \dot{m}_{AN,H_2}^{react} \Delta H^{react} \quad (42)$$

where ΔH^{react} is the lower heating value of the fuel [3,8–9]. The convective heat transfer to ambient air and to coolant water is:

$$\dot{Q}_{AMB}^{conv} = (hA)_{AMB}(T_M - T_{AMB}) \quad (43)$$

$$\dot{Q}_{CL}^{conv} = (hA)_{CL} \Delta T_{lm} = \dot{m}_{CL} c_{p,L}(T_{CL}^O - T_{CL}^I) \quad (44)$$

where $(hA)_{CL}$ and $(hA)_{AMB}$ are the heat convection coefficients of the cooling water, ΔT_{lm} is the log mean temperature difference between coolant inlet and coolant outlet, and $\dot{m}_{CL}$ is the mass flow rate of the coolant [3,8–9]. The log mean temperature difference between coolant inlet and outlet is defined as follows:

$$\Delta T_{lm} = \frac{\Delta T_{CL}^O - \Delta T_{CL}^I}{\ln(\Delta T_{CL}^O / \Delta T_{CL}^I)} \quad (45)$$

$$\Delta T_{CL}^O = T_m - T_{CL}^O, \qquad \Delta T_{CL}^I = T_m - T_{CL}^I \quad (46)$$

When liquid water exists in the channel, it tends to be on the channel surface. Since the heat transfer rate between the liquid water droplets and the MEA is always greater than that between the liquid water droplets and the gas, it is assumed that the temperature of the liquid water and the MEA are equal. Therefore, it is assumed that the phase change occurs on the surface of the channel [6]. The latent heat transfer due to the phase change of water is given by:

$$\dot{Q}_{AN}^{latent} = \frac{\dot{m}_{AN}^{vapor} H^{vapor}}{M_{H_2O}}, \qquad \dot{Q}_{CA}^{latent} = \frac{\dot{m}_{CA}^{vapor} H^{vapor}}{M_{H_2O}} \quad (47)$$

The term $\dot{W}_M^{elec}$ represents the electric power converted from the electrochemical reaction with n_{cell} single cells, each of area A [3].

$$\dot{W}_M^{elec} = -V_{cell} \times n_{cell} \times i \times A \quad (48)$$

The energy transfer due to mass transfer across the boundary of the MEA is expressed as:

$$\sum \dot{m}_M^I h_M^I - \sum \dot{m}_M^O h_M^O = \dot{m}_{H_2}^{react} c_{p,H_2}(T_{AN} - T_0) + \dot{m}_{O_2}^{react} c_{p,O_2}(T_{CA} - T_0) + \dot{m}_V^{trans} c_{p,V}(T_{AN,V}^{trans} - T_0) - \dot{m}_V^{trans} c_{p,V}(T_{CA,V}^{trans} - T_0) \quad (49)$$

Table 1
Thermodynamic constants

Parameter	Value	Parameter	Value
$\bar{R}$	8.314 kJ kmol^{-1} K	c_{v,O_2}	0.668 kJ kg^{-1} K
F	96,485	c_{v,N_2}	0.744 kJ kg^{-1} K
c_{p,H_2}	14.472 kJ kg^{-1} K	$c_{v,V}$	1.419 kJ kg^{-1} K
c_{p,O_2}	0.928 kJ kg^{-1} K	M_{H_2}	2.016 kg kmol^{-1}
c_{p,N_2}	1.041 kJ kg^{-1} K	M_{O_2}	32 kg kmol^{-1}
$c_{p,V}$	1.881 kJ kg^{-1} K	M_{N_2}	28 kg kmol^{-1}
$c_{p,L}$	4.184 kJ kg^{-1} K	M_{H_2O}	18.02 kg kmol^{-1}
c_{v,H_2}	10.302 kJ kg^{-1} K	ΔH^{react}	285.84 kJ mol^{-1}

The time rate of change of the MEA temperature is:

$$\frac{dT_M}{dt} = \frac{\dot{Q}_M^{CV} + \dot{W}_M^{elec} + \sum \dot{m}_M^I h_M^I - \sum \dot{m}_M^O h_M^O}{m_M c_{p,M}} \quad (50)$$

Parameters adopted for thermodynamic properties of species are summarized in Table 1. The specific heats of species and gas constants are collected from some published papers.

4. Simulation results and discussion

The PEFC stack is a multi-input and -output system. The inputs of the model are mass flow rate, relative humidity, and inlet gas temperature. The flow rate and temperature of the cooling water are the inputs of the model that determine the operating conditions. Simulation results show the effects of varying the inputs of the stack system. In this section, the simultaneous effects of temperature, humidity and pressure are elucidated using simulation results. Every operating condition except for electric load current is fixed. The relative humidity of each channel is set to 100% and the flow rate and temperature of cooling water are set to 50 L per min and 40 °C, respectively. The hydrogen gas feed is fixed to 1.371×10^{-4} g s^{-1} which is 1.5 times the stoichiometric hydrogen flow rate corresponding to a current load of 250 A. The air feed for the cathode is set to 6.539×10^{-3} g s^{-1}, i.e., twice the stoichiometric air flow rate corresponding to a current load of 250 A. The anode inlet and cathode inlet gases are set to 65 °C and are humidified to a relative humidity of 100% corresponding to the inlet gas temperature.

Table 2 shows the parameters used for the simulation. These parameters, such as cell count, channel volume, and heat con-

Table 2
Parameters dependent on the stack design

Parameter	Value	References
n_{cell}	35	[8]
t_m (cm)	0.0175	[4]
V_{AN} (m^3)	0.005	[5]
V_{CA} (m^3)	0.01	[5]
$(hA)_{AN}$ (kW K^{-1})	2×10^{-3}	[8]
$(hA)_{CA}$ (kW K^{-1})	10×10^{-3}	[8]
$(hA)_{AMB}$ (kW K^{-1})	17×10^{-3}	[8]
$(hA)_{CL}$ (kW K^{-1})	181.8×10^{-3}	[8]
$m_M c_{p,M}$ (kJ K^{-1})	35	[3]

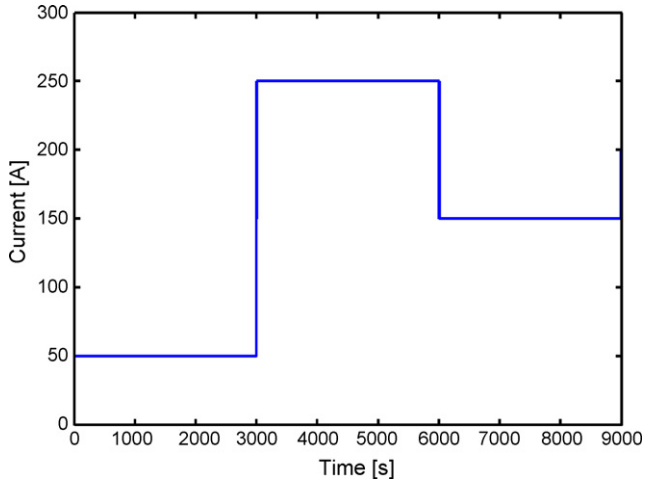

Fig. 5. Electric load current.

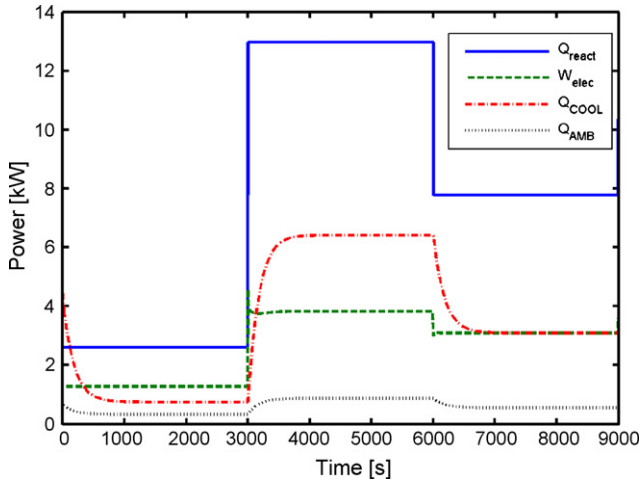

Fig. 7. Total reaction energy rate, output electric power, and heat dissipation with anode inlet RH 100% and cathode inlet RH 100% at 65 °C.

vection coefficients are related to stack design, and they may be adjusted to model the stack. The membrane thickness is determined assuming that the membrane is Nafion 117. In the MEA model, this assumption is valid, because a membrane hydration model and water transport mechanisms that are fitted to Nafion 117 are adopted.

Fig. 5 shows the electric load current, while Fig. 6 shows the relationship between the temperature and stack current variations. The MEA temperature as the equal to the stack temperature corresponding to the heat capacity of a PEFC stack. When the load current increases from 50 to 250 A, as in Fig. 5, the stack temperature increases above 75 °C. At the same time, the convective heat transfer between the MEA and the channel increases, and the increment of convective heat transfer crucially affects the channel temperature. The anode and cathode channel temperatures rapidly rise. When the load current decreases from 250 to 150 A, as in Fig. 5, at 6000 s, the stack temperature rapidly decreases to around 57 °C. This decrease in temperature occurs because of the reduction of heat generation due to the

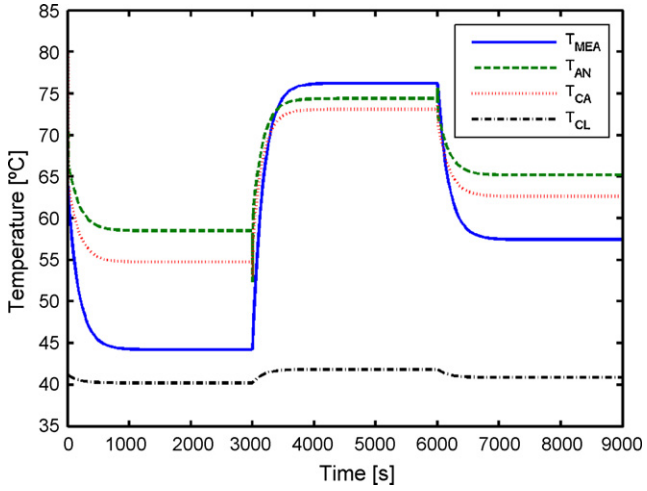

Fig. 6. Temperature variation with anode inlet RH 100% and cathode inlet RH 100% at 65 °C.

reaction and to irreversible losses such as Ohmic loss, activation and concentration losses.

The reduction of power generation by the electrochemical reaction occurs at 6000 s in Fig. 7, and the effects of irreversible losses are discussed later. As the temperature of the stack changes, the temperature of the cooling water exiting the stack also changes due to difference between the inlet cooling water and stack temperature. The convective heat transfer by the cooling water accounts for a large portion of power dissipation compared with other factors such as convective heat transfer to ambient air and power converted to electricity. The convective heat transfer by water cooling is, in particular, more significant than the electric power output from the PEFC at high load currents. These facts show that the increase of irreversible losses reduces the efficiency of the PEFC under higher current loads.

If the load current increases, the cell voltage decreases at 3000 s (Fig. 8). The unit cell voltage decreases after 3000 s. Although activation losses become smaller due to increasing temperature, the Ohmic and concentration losses increase and they have the main effect on the decrease of the cell voltage from 0.73 to 0.44 V. After 4000 s, when the load current decreases, the voltage output increases to 0.59 V because of the reduction in electric load current, which reduces the Ohmic losses and concentration losses. In the Fig. 8, the open-circuit voltage of the unit cell varies little with changes in the electric load current: This change is negligible compared with that of other losses. The change in Ohmic loss during the period of constant load current (4000–6000 s) is definitely larger than the changes in activation and concentration losses. Ohmic loss is sensitive to the membrane water content which is, in turn, mainly affected by the relative humidity of inlet gas and the membrane temperature.

Fig. 9 shows the transition of membrane water content during operation using fully humidified feed gas. The membrane water content is determined by the amount of water surrounding the membrane and the membrane temperature. In the previous section, the relationship between membrane water content and membrane temperature was presented as a function of water

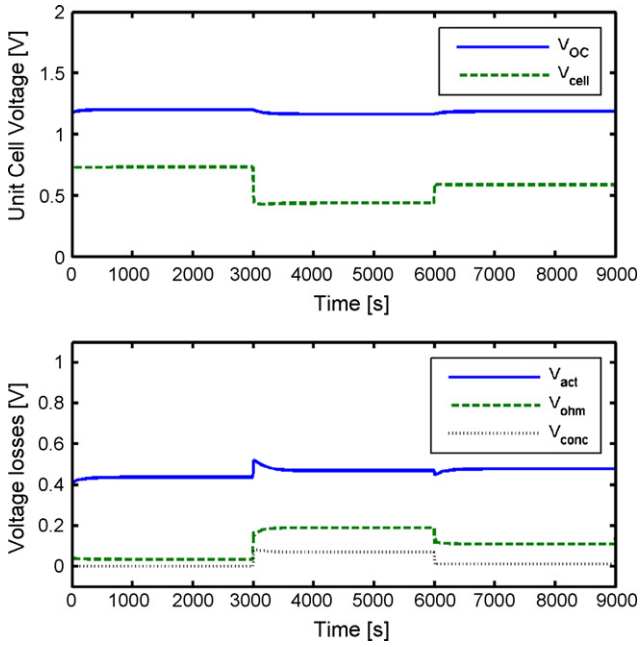

Fig. 8. Unit cell voltage and voltage losses with anode inlet RH 100% and cathode inlet RH 100% at 65 °C.

activity, which is determined by the membrane temperature and the water vapour pressure on both sides. When the PEFC operates at a load current of 50 A, the membrane temperature is below 45 °C, so that the amount of water produced and supplied is sufficient to hydrate the membrane. When the PEFC operates at high load current (250 A), the temperature of the MEA rises to 75 °C, as shown in Fig. 6. Thus, the membrane water content becomes around 14.4 (Fig. 9). During this stage, the membrane water content decreases as the MEA temperature increases, which affects the reference state of the water, namely, the water saturation pressure. After 4000 s, the load current is reduced to 150 A, as shown in Fig. 5. The decrease of water production which occurs because of the decrease of load current causes an under-shoot of the membrane water content for a short time. After this under-shoot, the water content rebounds because the MEA temperature decreases. In this model, the water content shows the dynamic behaviour determined by the change in membrane temperature. The simulation shows that suitable water and thermal management are needed simultaneously.

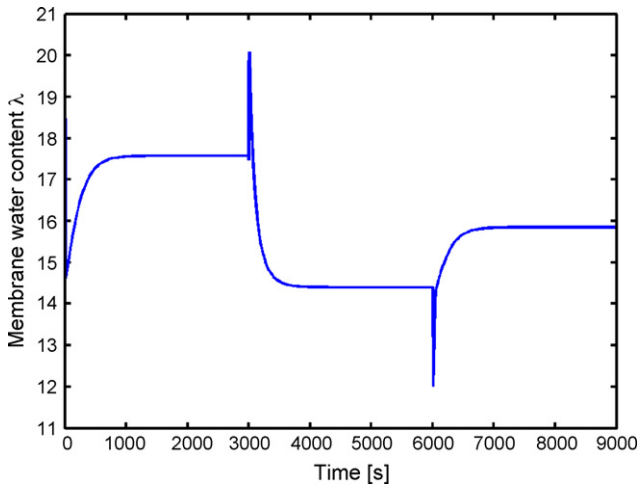

Fig. 9. Membrane water content with anode inlet RH 100% and cathode inlet RH 100% at 65 °C.

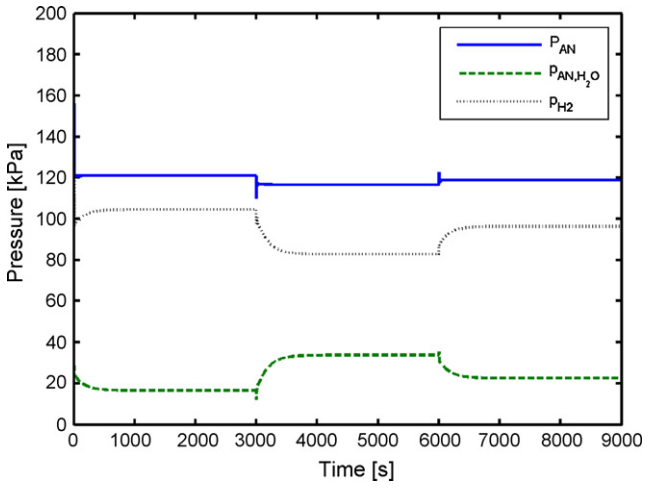

Fig. 10. Pressure of gas in anode channel with anode inlet RH 100% and cathode inlet RH 100% at 65 °C.

Another important operating condition is channel pressure. The partial pressures of the species in the channel are determined by the mass continuity and the Ideal Gas Law. In this study, all of gas species are modelled using the Ideal Gas Law. Figs. 10 and 11 present the pressure in the anode and cathode channels, respectively. The change in the total pressure in each channel is unremarkable because it is assumed that the flow rate of the exhaust gas is proportional to the channel pressure and that the inlet flow rate is constant. The channel pressure changes slightly because of the transport of water across the MEA. On the other hand, the partial pressures of species such as water vapour, hydrogen, oxygen and nitrogen exhibit relatively large variations. If the water vapour is saturated, the phase of water changes from vapour to liquid based on the channel temperature. Thus, an increase in channel tempera-

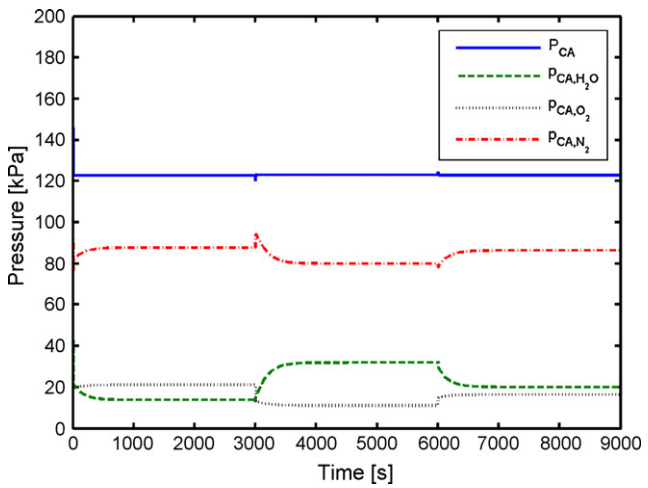

Fig. 11. Pressure of gas in cathode channel with anode inlet RH 100% and cathode inlet RH 100% at 65 °C.

ture causes an increase in vapour pressure. Fig. 10 shows that change in of water vapour pressure in anode channel follows a similar trend to the change in the anode channel temperature.

Fig. 11 gives the pressure in the cathode channel and the partial pressures of the involved species, namely, oxygen, nitrogen, and water vapour. In the cathode channel, the water vapour pressure varies with the cathode channel temperature. Conversely, the partial pressures of the other species such as oxygen, and nitrogen vary inversely with vapour pressure. Although the partial pressures of hydrogen, oxygen, and nitrogen in the channel are also affected by the temperature (per the Ideal Gas Law), the amounts of these species decrease with increasing quantities of exhaust gas due to the difference between the channel and ambient pressures.

In the case of water vapour, liquid water is present in the channel (Fig. 12), that is, the vapour pressure is determined only by the relationship between saturation vapour pressure and temperature under this operating condition.

The net water transport across the channel is from the cathode to the anode side. The upper graph of Fig. 13 plots the direction and amount of the net water transport across the membrane. The lower graph in Fig. 13 shows that during increase in the load current, the electro-osmotic drag suddenly increases up to $4 \times 10^{-3}\,\mathrm{kg\,s^{-1}}$, and the convective water flows due to the pressure gradient increase simultaneously in the opposite direction. A negative sign indicates that the water moves from the cathode to the anode channel. Water transport from the cathode to the anode side assists the water management of the fuel cell, because it prevents the drying out of the anode-side membrane by electro-osmotic drag. After an increase in the electro-osmotic drag occurs, the magnitudes of the electro-osmotic drag and the convection by pressure gradients decrease to around $3 \times 10^{-3}\,\mathrm{kg\,s^{-1}}$. The slow change of the MEA temperature affects the membrane water content, which in turn determines the electro-osmotic, water transport and diffusion coefficients. The diffusion of the water is relatively small compared with the electro-osmotic drag and convection by the pressure gradient.

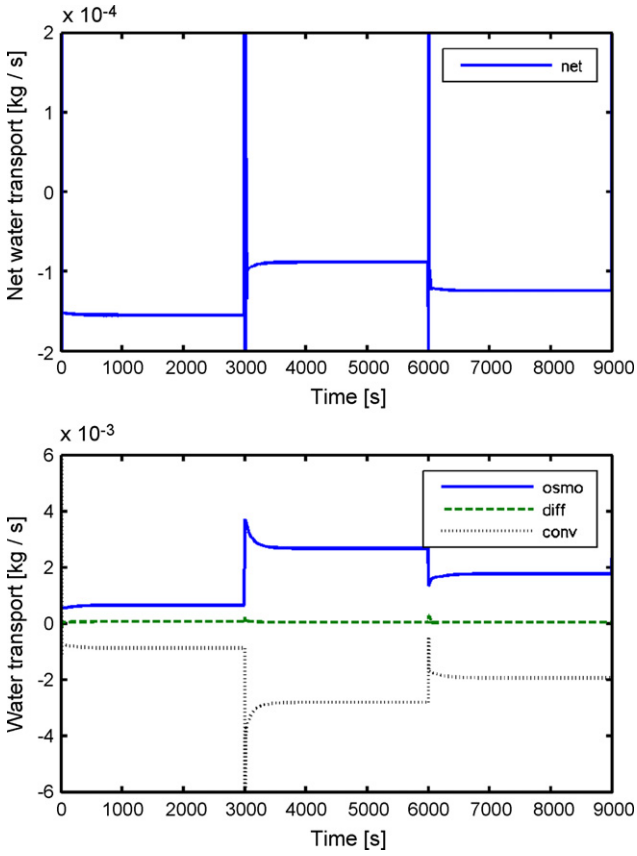

Fig. 13. Water transport across MEA with anode inlet RH 100% and cathode inlet RH 100% at 65 °C.

The simulation was conducted again by changing the inlet humidity condition. The relative humidity of the inlet gas was set to 75% at a 65 °C dew point. Fig. 14 plots the dependence of temperature on humidity. Compared with Fig. 6, the stack temperature increases to 78.4 °C at a load current of 250 A, due to an increase in Ohmic loss. The increase in Ohmic loss causes an increase in the heat converted from the produced power due to the electrochemical reaction instead of electric power. Low humid-

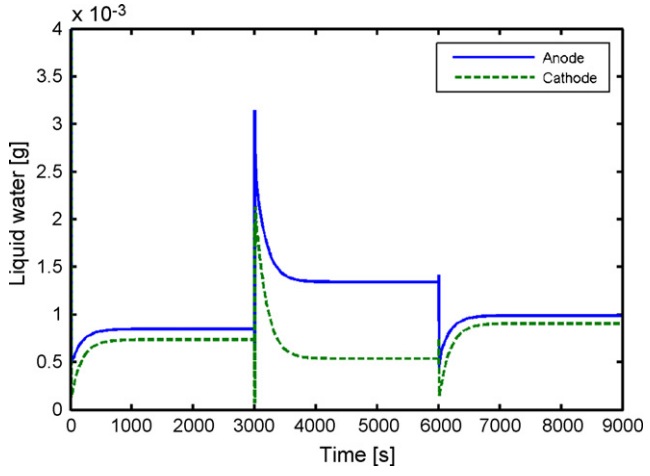

Fig. 12. Liquid water in the anode channel and cathode channel with anode inlet RH 100% and cathode inlet RH 100% at 65 °C.

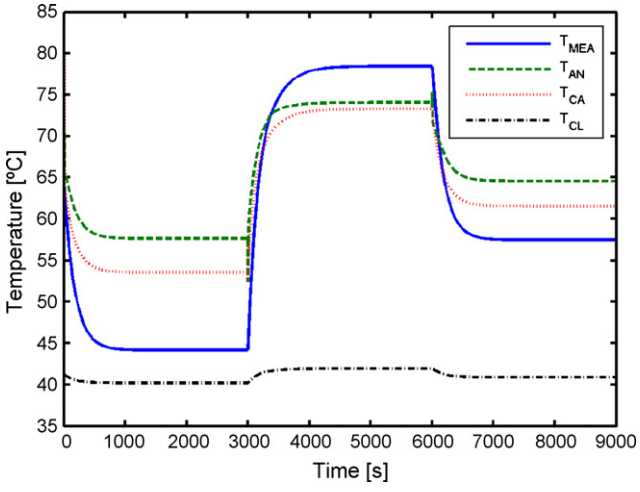

Fig. 14. Temperature variation with anode inlet RH 75% and cathode inlet RH 75% at 65 °C.

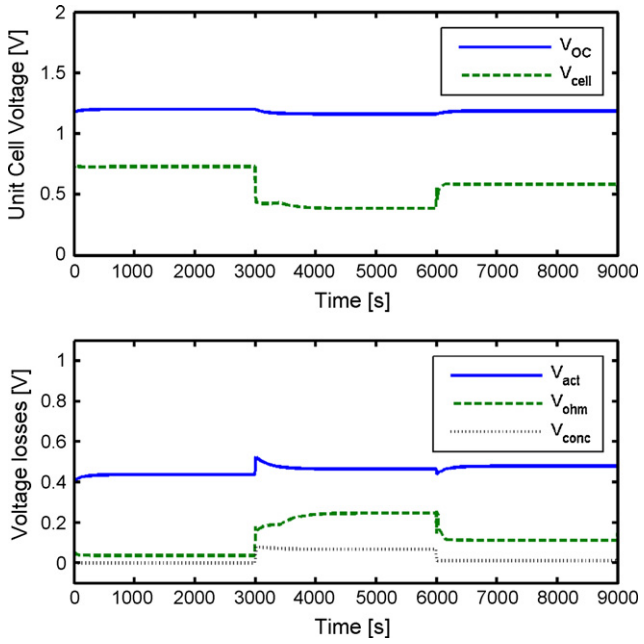

Fig. 15. Unit cell voltage and voltage losses with anode inlet RH 75% and cathode inlet RH 75% at 65 °C.

ity causes a decrease in the membrane conductivity and hence an increase in Ohmic loss, as illustrated in Fig. 15. The lower graph shows the increase in Ohmic loss due to low humidity as well as the time-varying Ohmic loss due to the increase in stack temperature under a current load of 250 A (Fig. 14). Under fixed humidity conditions, the membrane humidity level is higher at higher temperatures.

The water content reported in Fig. 16 is smaller than that in Fig. 9, because the inlet gas has a lower humidity. In the transient region, the graph does not vary smoothly near a water content of 14 because the relationship between water activity and water content is changed near that point due to Eq. (28). The relationship between water activity and membrane water content above the vapour saturation level is not correctly correlated in the literature. In this model, the Ohmic loss and stack temperature recursively influence each other through the membrane water content and water activity. To avoid an increase in Ohmic loss under low-humidity conditions, the temperature of the cooling water should be controlled. Fig. 17 shows reversibilities of the stack at a cooling water inlet temperature of 35 °C.

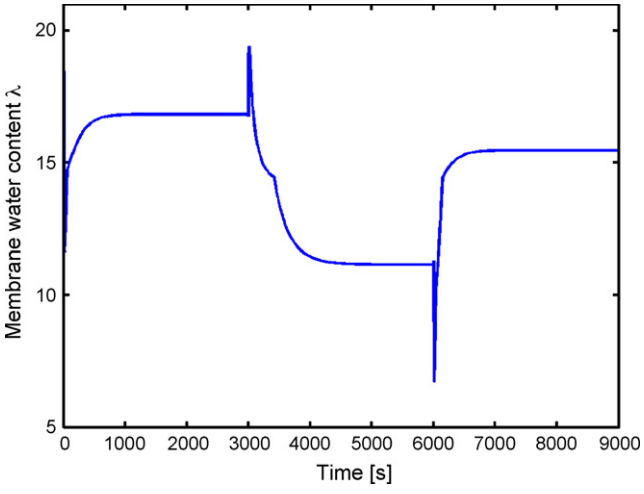

Fig. 16. Membrane water content with anode inlet RH 75% and cathode inlet RH 75% at 65 °C.

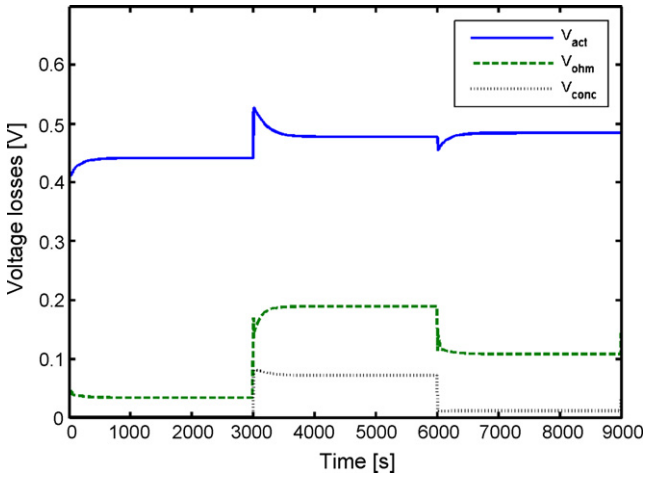

Fig. 17. Unit cell voltage and voltage losses with anode inlet RH 75%, cathode inlet RH 75% at 65 °C and a cooling water temperature of 35 °C.

Cooling water at a low temperature aids in the water management of the stack. A low inlet cooling water temperature improves exhausting heat and regulating stack temperature. At low temperatures, a relatively small amount of water feed through the inlet gas is sufficient to hydrate the membrane, thus increasing conductivity. The Ohmic loss is therefore less than that when the cooling water is at 40 °C (Fig. 17). In order to operate the PEFC stack under optimum conditions, external humidification and cooling water temperature should be applied simultaneously.

5. Summary and conclusions

In this study, a PEFC model structure, which consists of three control volumes, is developed. The three control volumes are the anode, the cathode and the MEA control volumes. The mass conservation law and energy conservation law are applied to each control volume in order to model the flow dynamics and thermal behaviour of the species therein.

The simulation exhibits reasonable behaviour for the mass and energy flows within the PEFC. However, some simulation parameters from other literature are used [3–5,8]. In future studies, these parameters will be adjusted using experimental data. This lumped parameter model is mathematically simple but describes the essential states of the system that affect the performance of the PEFC, such as temperature, pressure and humidity. This modelling study is therefore useful for understanding interactions among control volumes and for designing model-based controllers for PEFC systems.

Acknowledgements

The work was supported by the Korea Science and Engineering Foundation (KOSEF) through the National Research Laboratory Program funded by the Ministry of Science and Technology (No. M1-0203-00-0058) and is part of the project "Development of Partial Zero Emission Technology for Future Vehicle" funded by Ministry of Commerce, Industry and Energy.

References

[1] P. Costamagna, S. Srinivasan, J. Power Sources 102 (2001) 242–252.
[2] P. Costamagna, S. Srinivasan, J. Power Sources 102 (2001) 253–269.
[3] X. Xue, J. Tang, A. Smirnova, R. England, N. Sammes, J. Power Sources 133 (2003) 188–204.
[4] T.E. Springer, T.A. Zawodzinski, S. Gottesfeld, J. Electrochem. Soc. 138 (1991) 2334–2342.
[5] J.T. Pukrushpan, A.G. Stefanopoulou, H. Peng, Trans. ASME 126 (2004) 14–25.
[6] J.S. Yi, T.V. Nguyen, J. Electrochem. Soc. 145 (1998) 1149–1159.
[7] J. Larminie, A. Dicks, Fuel Cell System Explained, second ed., John Wiley & Sons, England, 2000, pp. 396–400.
[8] J.C. Amphlett, R.F. Mann, B.A. Peppley, P.R. Roberge, A. Rodrigues, J. Power Sources 61 (1996) 183–188.
[9] F.P. Incropera, D.P. DeWitt, Fundamentals of Heat and Mass Transfer, fifth ed., John Wiley & Sons, 2002.
[10] J.P. Evans, Experimental Evaluation of the Effect of Inlet Gas Humidification on Fuel Cell Performance, Master Thesis, Virginia Technology, September 2003.
[11] X. Yu, B. Zhou, A. Sobiesiak, J. Power Sources 147 (2005) 184–195.
[12] A.Z. Weber, J. Newman, J. Electrochem. Soc. 150 (2003) 1008–1015.
[13] A.Z. Weber, J. Newman, J. Electrochem. Soc. 151 (2004) 311–325.
[14] A.Z. Weber, J. Newman, J. Electrochem. Soc. 151 (2004) 326–339.
[15] J.C. Amphlett, R.M. Baumert, R.F. Mann, B.A. Peppley, P.R. Roberge, J. Electrochem. Soc. 142 (1995) 1–8.
[16] J.C. Amphlett, R.M. Baumert, R.F. Mann, B.A. Peppley, P.R. Roberge, J. Electrochem. Soc. 142 (1995) 9–15.